Attempt to distinguish electric signals of a dichotomous nature

P. A. Varotsos,[1,2,*] N. V. Sarlis,[1] and E. S. Skordas[1,2]

[1]*Solid State Section, Physics Department, University of Athens, Panepistimiopolis, Zografos, Athens 157 84, Greece*
[2]*Solid Earth Physics Institute, Physics Department, University of Athens, Panepistimiopolis, Zografos, Athens 157 84, Greece*

Three types of electric signals were analyzed: Ion current fluctuations in membrane channels (ICFMC), Seismic electric signals activities (SES), and "artificial" noises (AN). The wavelet transform, when applied to the conventional time domain, does not allow a classification of these signals, but does so in the "natural" time domain. A classification also becomes possible, if we study $\langle \chi^q \rangle - \langle \chi \rangle^q$ versus q, where χ stands for the "natural" time. For q values approximately between 1 and 2 the signals are classified and ICFMC lies between the other two types. For $q=1$, the "entropy" $S \equiv \langle \chi \ln \chi \rangle - \langle \chi \rangle \ln \langle \chi \rangle$ of ICFMC almost equals that of a "uniform" distribution, while the AN and SES have larger and smaller S values, respectively. The recent [P. Varotsos, N. Sarlis, and E. Skordas, Phys. Rev. E **67**, 021109 (2003)] finding that, in short time scales, both SES and AN (which are shown to be non-Markovian) result in comparable detrended fluctuation analysis exponents $\alpha \in (1.0, 1.5)$ is revisited. Even a Markovian dichotomous time series, in short time scales, leads to similar α exponents.

I. INTRODUCTION

Single ionic channels in a membrane open and close spontaneously in a stochastic way, resulting in current and voltage changes, which resemble the realizations of random telegraph signals, RTS (see Refs. [1,2], and references therein). A second type of signals, which have also an RTS feature, are the so-called seismic electric signals (SES) activities. These are low frequency (≤ 1 Hz) changes of the electric field of the earth that have been found in Greece [3–7] and Japan [8,9] to precede earthquakes with lead times ranging from several hours to a few months. It has been suggested [3] that SES activities are emitted when a *critical* stress is approached in the focal area. Beyond the SES activities, however, the data collection system (sampling rate $f_{exp} = 1$ Hz) also records "artificial" noises (AN), i.e., electrical disturbances due to nearby man-made electrical sources. Figure 1 shows excerpts of a number of these three types of signals, i.e., ICFMC (ion current fluctuations in membrane channels), SES activities and AN (they are presented in normalized units, i.e., by subtracting the mean μ and dividing by the standard deviation σ). The latter have been intentionally selected [10] to exhibit a RTS feature similar to that of SES activities. This RTS feature allows us to construct [10] the time series of subsequently high-level (T_h) and low-level (T_l) durations (dwell times) $\{T_{h,j}\}_{j=1}^{N_h}$, $\{T_{l,j}\}_{j=1}^{N_l}$, where N_h and $N_l (=N_h - 1)$ are the total number of the high- and low-level states' durations [11], respectively.

In previous publications, various statistical methods (e.g., Hurst and detrended fluctuation analysis, DFA) lead to power-law exponents, which are consistent with long-range correlations for both SES activities [12] and AN [10], as earlier found [13] for ICFMC. Aiming at the classification of these three types of electric signals, a power spectrum analysis in the "natural" time domain (see below) was also made and led to the following results [10]: In the low frequency range, it seems that certain power spectrum characteristics distinguish SES activities from AN, while ICFMC lie in the boundary between the other two types of signals. The natural time χ is introduced [5,12] by ascribing to the kth pulse of an electric signal (Fig. 1), consisting of N pulses, the value $\chi_k = k/N$ and the analysis is made in terms of the couple (χ_k, Q_k) where Q_k stands for the duration of the kth pulse. The quantity Q_k is the so-called dwell time, but for the high-level *only*, $Q_k = T_{h,k}$. Figure 2 shows how the electric signals of Fig. 1 are read in the natural time, i.e., p_k or $p(\chi)$ versus χ_k or χ, respectively, where $p_k = Q_k / \Sigma_{n=1}^{N} Q_n$.

Since the power spectrum and the correlation analysis (the conventional DFA) can measure only one exponent, these methods are more suitable for the investigation of monofractal signals. In several cases, however, the records cannot be accounted for by a single scaling exponent (i.e., do not exhibit a simple monofractal behavior). Recall [14–17] that the
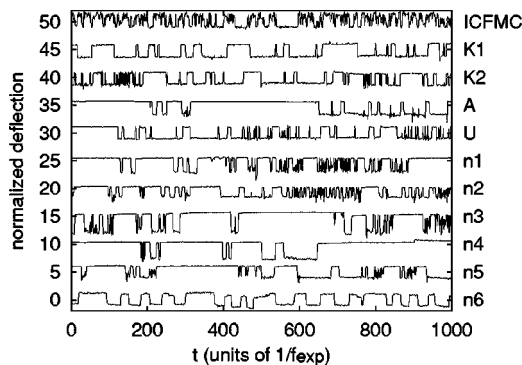

FIG. 1. Excerpts of ICFMC ($f_{exp} = 10$ kHz), four SES activities, labeled $K1$, $K2$, A, U, and six artificial noises, labeled $n1$–$n6$ ($f_{exp} = 1$ Hz). The signals are presented in normalized units, i.e., by subtracting the mean value μ and dividing by σ (see the text). For the sake of clarity, all signals (except of $n6$) are displaced vertically by constant factors.
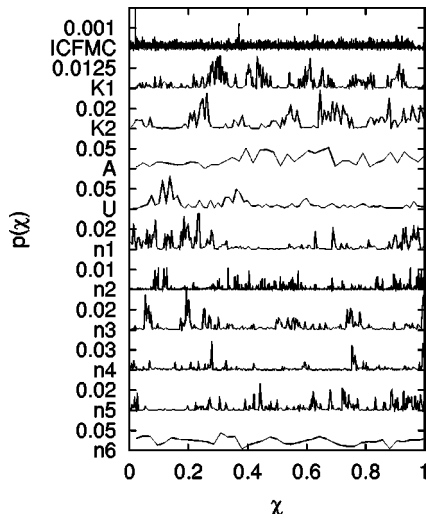
*Electronic address: pvaro@otenet.gr

FIG. 2. The signals of Fig. 1, but read in the natural time domain (for $p(\chi)$ see also Refs. [5,12]).

root mean square variability of the detrended process in DFA varies with scale l as $F_{DFA}(l) \sim l^\alpha$. In some examples, there exist crossover (time) scales separating regimes with different scaling exponents. This was the case of the SES activities in Ref. [12] (see their Fig. 6) which reported different DFA exponents for times Δt smaller than around 30 s and larger than ≈ 30 s (Fig. 3) (i.e, $\alpha \approx 1.2$ and 0.9, respectively). This point was found necessary to be revisited in this paper in order to elucidate the possible origin of the DFA behavior at the short time scales. In general, if a multitude of scaling exponents is required for a full description of the scaling behavior, a multifractal analysis must be applied (e.g., Ref. [18], and references therein). A multifractal analysis can be performed by the wavelet transform (e.g., [19–22]) as well as by the multifractal detrended fluctuation analysis [23,24] (MF-DFA). In MF-DFA [24], the qth order fluctuation function $F_q(l)$ scales as $F_q(l) \sim l^{h(q)}$, where the function $h(q)$ is
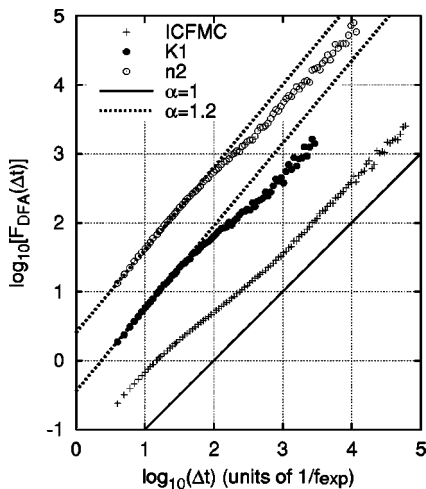

FIG. 3. The DFA analysis for three indicative signals mentioned in Fig. 1. The continuous straight line corresponds to $\alpha = 1$ and is drawn for the sake of convenience. The dotted straight lines correspond to $\alpha = 1.2$.

called generalized Hurst exponent. For stationary time series, $h(2)$ is identical [24] to the well known Hurst exponent H, i.e., $h(2) = H$. For monofractal time series $h(q)$ is independent of q, while for multifractal series $h(q)$ depends on q. MF-DFA was recently applied [10] to the time series of SES activities and AN. This multifractal analysis, when carried out in the conventional time frame, did not lead to any distinction between these two types of signals. On the other hand, if the analysis is made in the natural time domain, a distinction becomes possible [10]. One of the aims of the present paper is to investigate whether this holds, if wavelet transform, instead of MF-DFA, is employed.

Beyond the two points mentioned above, the present paper aims, in general, at the classification of the three types of signals, which although look to be similar, they are emitted from systems of different dynamics. More specifically, it provides an attempt to find rules in order to distinguish (true) SES activities from AN, which is practically an important problem. The parallel study of ICFMC is motivated by the aforementioned finding [10] that the power spectrum analysis in the natural time domain reveals that ICFMC lie—very close to a uniform distribution and—in the boundary between the other two types of signals.

The present paper is organized as follows: In Sec. II, DFA is revisited in order to shed light on the exponent $\alpha \approx 1.2$ that has been found in short scales for both SES activities and AN. These two types of signals are studied in Sec. III by applying the wavelet transform. In Secs. IV and V, we show that the fluctuation function $\langle \chi^q \rangle - \langle \chi \rangle^q$ and the "entropy" $\langle \chi^q \ln \chi \rangle - \langle \chi \rangle^q \ln \langle \chi \rangle$ may serve for the classification of the three types of signals. Sec. VI is reserved for a short discussion of the results, while the conclusions are summarized in Sec. VII.

II. DETRENDED FLUCTUATION ANALYSIS REVISITED

The relation between F_{DFA} and the power spectral density $S(\omega)$ is given by [16]

$$F_{DFA}^2(l) = \frac{l}{2\pi} \int_0^\infty S(w/l) r_{DFA}(w) dw, \qquad (1)$$

where w denotes the *dimensionless* frequency and $r_{DFA}(w)$ is given from [16]

$$r_{DFA}(w) = [w^4 - 8w^2 - 24 - 4w^2 \cos(w) + 24 \cos(w)$$
$$+ 24w \sin(w)]/w^6. \qquad (2)$$

In a Markovian dichotomous time series the probability densities (dwell-time distributions) for the time spent in a single sojourn in the states "high" and "low," respectively, are both exponential, i.e., $p_1(T) \propto \exp(-T/\tau_{high})$, $p_2(T) \propto \exp(-T/\tau_{low})$, whereas the field-field conditional probabilities vary [25] exponentially with a "relaxation" time $\tau_{eff}, 1/\tau_{eff} \equiv 1/\tau_{high} + 1/\tau_{low}$ (see also Ref. [11]). Assuming that the states low and high have amplitudes 0 and ΔE, we find [11]
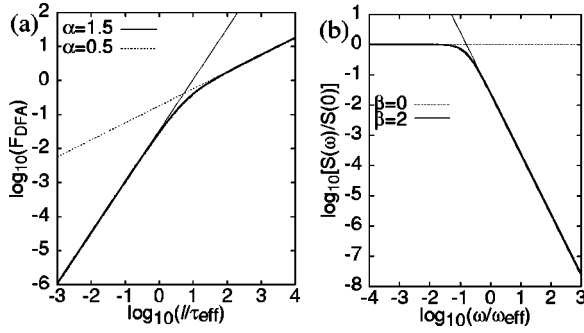
FIG. 4. The case of a Markovian dichotomous signal: (a) the variability measure F_{DFA} (thick line, in units of ΔE) vs l/τ_{eff} and (b) the normalized power spectral density $S(\omega)/S(0)$ (thick line) vs ω/ω_{eff}. The thin straight continuous (dotted) lines correspond to the short (long) time ranges.

$$S(\omega) = \frac{4(\Delta E)^2 \tau_{eff}^2}{(\tau_{low} + \tau_{high})(1 + \omega^2 \tau_{eff}^2)}. \tag{3}$$

Using Eqs. (1)–(3), we plot in Fig. 4(a), the $F_{DFA}(l)$ versus l/τ_{eff} for a dichotomous Markovian process, while Fig. 4(b) depicts $S(\omega)$ versus ω/ω_{eff} where $\omega_{eff} \equiv 2\pi/\tau_{eff}$, using Eq. (3). Concerning the DFA exponent α, Fig. 4(a) shows the following:

(i) For short time scales (high frequencies), i.e., $\Delta t \ll \tau_{eff}$, the DFA exponent approaches the value $\alpha = 1.5$. (Note that such a behavior is expected for any signal with a high frequency spectrum as given in Eq. (3), see below.)

(ii) For large time scales (low frequencies), i.e., $\Delta t \gg \tau_{eff}$, we find $\alpha = 0.5$, as expected.

(iii) For intermediate scales, comparable to τ_{eff}, DFA exponents exceeding unity (e.g., 1.2 or so) naturally emerge.

Recall that the points above hold in the conventional time frame. If the analysis is performed in the natural time domain (cf. considering as "high" either of the two states in the Markovian series), we find DFA exponent $\alpha = 0.5$ [e.g., Fig. 5(b)] and power spectrum exponent $\beta = 0$. These values may elucidate the Markovian nature of the time series, avoiding
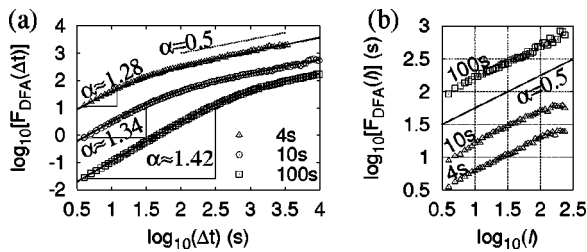

FIG. 5. (a) The variability measure $F_{DFA}(\Delta t)$ (in units of ΔE) for three Markovian dichotomous time-series, calculated with $\tau_{eff} = 4$ (triangles), 10 (open circles), and 100 s (open squares). The continuous lines, in each case, correspond to the theoretical estimation described in Sec. II. (b) Same as in (a), but calculated when the time series are read in the natural time domain. The straight lines [dotted in (a), solid in (b) correspond to $\alpha = 0.5$]. The curves are shifted relative to each other by constant factors.

the existence of the aforementioned characteristic intermediate scaling regions that appear in the conventional time frame.

We now turn to the appearance of the crossover at $\Delta t \approx 30$ s for both the SES activities and AN found in Ref. [10]. We first clarify that these signals are non-Markovian (and their long-range correlations mainly arise from their dichotomous nature [10,12]). Here their non-Markovianity was further investigated by calculating [11] the (non-Markovian) quantitative global measure G, as defined in Ref. [1]. As an example, for the cases $K1$ and $n1$, we found [11] G values that exceed by one order of magnitude the corresponding G values for computer-generated Markovian dichotomous series of comparable length. This suggests the non-Markovian character of the experimental data. The non-Markovianity of both SES activities and AN was also investigated by means of the dwell-time distributions: The cumulants σ^2/μ^2, *skewness*, and *kurtosis* were calculated [11] for the series of the high-(T_h) and low-(T_l) level states' durations for all the SES activities and AN; the resulting values show [11] that none of the time series could be compatible with an exponential (dwell-time) distribution and hence Markovian. We now define for non-Markovian time series the quantity $\langle T \rangle$ in an analogous way with the quantity τ_{eff} introduced above for the Markovian ones, i.e., $1/\langle T \rangle \equiv 1/\langle T_h \rangle + 1/\langle T_l \rangle$. These values of $\langle T \rangle$ for all SES activities and AN mentioned in Fig. 1, are given in Ref. [11]. In Fig. 5(a), we give examples of DFA plots for Markovian time series that have various values of τ_{eff}, two of which ($\tau_{eff} = 4$ s and 10 s, upper two curves) have been intentionally selected to be comparable with $\langle T \rangle$ of the SES activities and AN. We note that a crossover occurs almost at the *same* region (with almost the *same* α exponents at the short scales *only*) for the upper two curves of both Figs. 3 and 5(a). In other words, in short time scales, even Markovian dichotomous time series (that have τ_{eff} values comparable to $\langle T \rangle$ of the SES activities and AN) result in α values in the range $1 \leq \alpha \leq 1.5$ (with a crossover at $\Delta t \approx 30$ s). More generally, we can state that not only signals of dichotomous nature, but any signal with a high frequency spectrum as given in Eq. (3) will lead to the same scaling behavior of $F_{DFA}(\Delta t)$ for small time lags Δt (irrespectively of the particular shape of the signal; for example, a Gaussian signal with this spectrum will be much smoother and will display a continuity of values rather than only two steps).

III. THE WAVELET TRANSFORM

We start with the application of the continuous wavelet transform to the original time series of the SES activities and AN depicted in Fig. 1. As an example, we present in Fig. 6 the results of the wavelet transform modulus maxima (WTMM) method that was applied [11], using the LASTWAVE [26] software and the g_4 wavelet (i.e., the fourth derivative of the Gaussian [11]). An inspection of Fig. 6 reveals that the curves showing the q dependence of $h(q)$: (i) suggest the multifractal character of both types of signals and (ii) are not classified, thus not allowing any obvious distinction between SES activities and AN.

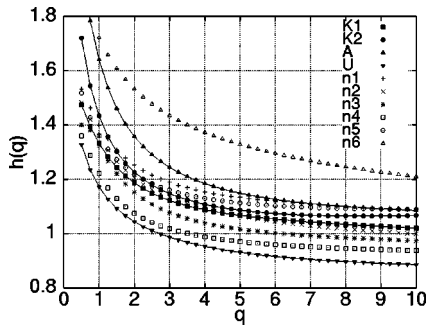The same conclusion is drawn [see Fig. 7(a)] if we apply

FIG. 6. The q dependence of the generalized Hurst exponent $h(q)$, resulting from the application of the WTMM method using a g_4 wavelet [11]. For the sake of clarity, the continuous curves correspond to the four SES activities (bold symbols), while for AN thinner symbols were used.

the orthogonal wavelet transform analysis [11] to the time series of the signals mentioned in Fig. 1. This analysis was made with the program provided by Veitch *et al.* [27], using a Daubechies 1 (i.e., Haar) wavelet [28]. In summary, the
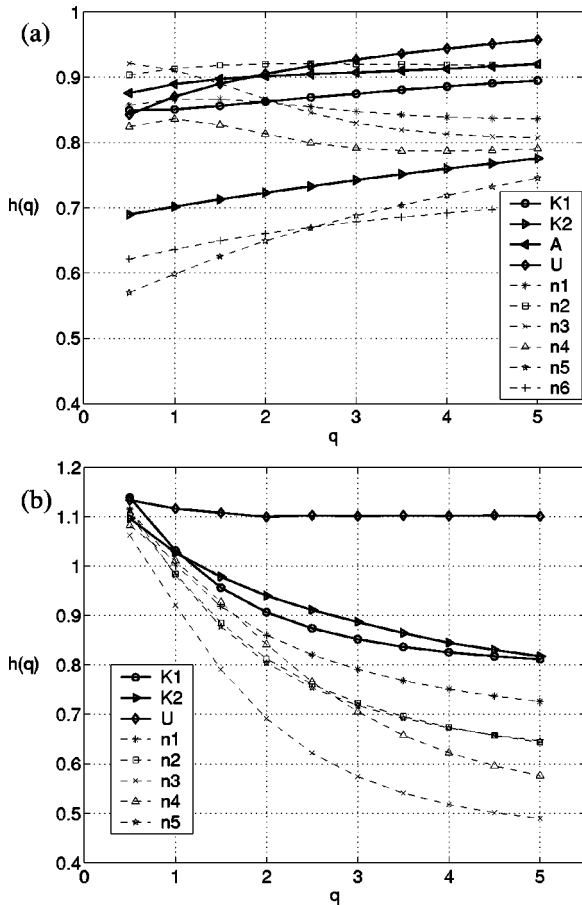

FIG. 7. The q dependence of the generalized Hurst exponent $h(q)$ resulting from the orthogonal wavelet transform analysis [11] using a Daubechies 1 wavelet. The continuous curves correspond to the SES activities and the broken to AN: (a) of the original time series (Fig. 1) and (b) of the series read in the natural time domain (Fig. 2). Note that the signals A and $n6$ could not be analyzed in the natural time domain due to the small number of data points.
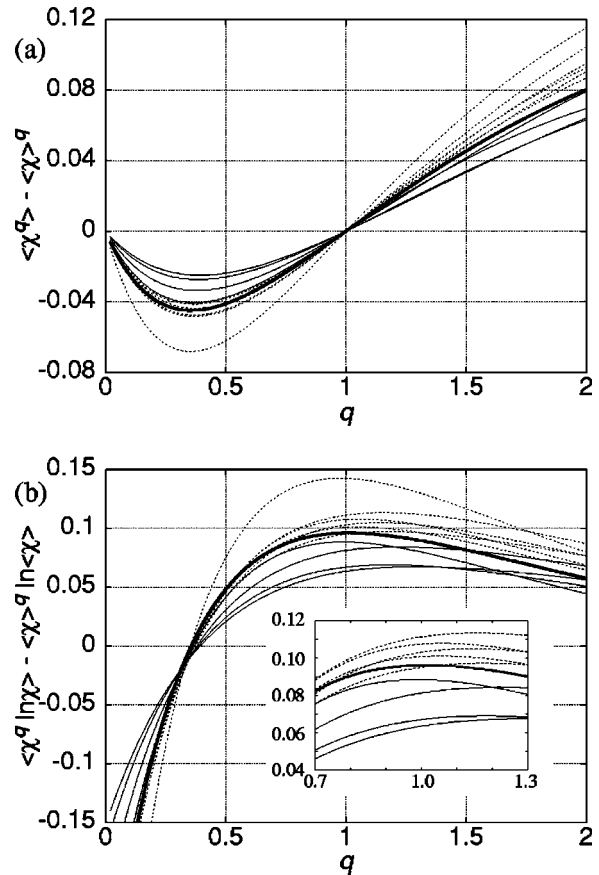

FIG. 8. (a) and (b) correspond to the function $\langle \chi^q \rangle - \langle \chi \rangle^q$ and its derivative $\langle \chi^q \ln\chi \rangle - \langle \chi \rangle^q \ln\langle \chi \rangle$ with respect to q, vs q. ICFMC—thick continuous line; SES activities—thin solid lines; AN—broken lines. The uncertainties, for $q=2$ in (a) and for $q=1$ in (b) are given in Table I.

wavelet transform analysis when applied to the conventional time frame does not seem to provide a distinction between SES activities and AN.

We now proceed to the application of the wavelet transform to the signals as they are read in the natural time domain (Fig. 2). The results of the orthogonal wavelet transform analysis (cf. WTMM could not be reliably applied in view of the small number of points), using again a Daubechies 1 wavelet [28], are depicted in Fig. 7(b). An inspection of these $h(q)$ versus q curves, in spite of the large estimation errors (see Table I), seems to show a classification as follows: For q values around 2 or larger the resulting h values for the SES activities are higher than those of the AN. In summary, the wavelet transform analysis allows a distinction between SES activities and AN *if* it is applied to the natural time domain.

IV. THE FLUCTUATION FUNCTION $\langle \chi^q \rangle - \langle \chi \rangle^q$

The qth order fluctuation function $\langle \chi^q \rangle - \langle \chi \rangle^q$ versus q, for all the electric signals, is depicted in Fig. 8(a), in the range $0 < q \leqslant 2$ (recall that [5] $\langle \chi^m \rangle = \Sigma_k \chi_k^m p_k$). This figure shows that the curves for the SES activities and AN, at least in the range $q \in (1,2]$, fall practically into two different

TABLE I. Summary of the results in the natural time-domain.

Signal	$h(2)$[a]	$h(2)$[b]	S	κ_1[c]
$K1$	0.98 ± 0.08	0.91 ± 0.10	0.067 ± 0.003	0.063 ± 0.003
$K2$	0.92 ± 0.10	0.94 ± 0.17	0.081 ± 0.003	0.078 ± 0.004
A	0.87 ± 0.27		0.070 ± 0.008	0.068 ± 0.004
U	0.98 ± 0.13	1.10 ± 0.27	0.092 ± 0.004	0.071 ± 0.004
ICFMC	0.86 ± 0.07[d]		0.096 ± 0.003	0.080 ± 0.003
Uniform			$\ln(2)/2-1/4$	$1/12$
$n1$	0.68 ± 0.07	0.86 ± 0.12	0.143 ± 0.003	0.115 ± 0.003
$n2$	0.79 ± 0.03	0.81 ± 0.05	0.103 ± 0.003	0.093 ± 0.003
$n3$	0.78 ± 0.06	0.69 ± 0.11	0.117 ± 0.010	0.100 ± 0.008
$n4$	0.76 ± 0.06	0.84 ± 0.13	0.106 ± 0.010	0.100 ± 0.013
$n5$	0.68 ± 0.05	0.77 ± 0.08	0.091 ± 0.011	0.086 ± 0.007
$n6$	0.78 ± 0.20		0.102 ± 0.007	0.084 ± 0.004

[a]From MF-DFA in the natural time domain.

[b]From the orthogonal wavelet transform in the natural time domain.

[c]From Ref. [10]. Note that $n1-n5$ correspond to $N1-N5$ and $n6$ to $N9$ (cf. the symbols $N1-N5$ and $N9$, instead of $n1-n6$, were used in Ref. [10]).

[d]This exponent corresponds to the closed states for ICFMC [32].

classes (thus allowing a distinction), while the ICFMC curve lies just between them. The results of SES activities, for $q=2$, scatter around the value [12]: $\kappa_1[\equiv\langle\chi^2\rangle-\langle\chi\rangle^2]=0.07$, obtained [5,12] from the theory of critical phenomena. The κ_1 value that corresponds to the ICFMC data is [12] 0.080 ± 0.003, while for the AN it is larger than around 0.083 [10]. The latter value ($\kappa_u=1/12\approx0.083$) is just that corresponding to a uniform (u) distribution for p_k (see Ref. [10]); thus, the difference $(1/12)-\kappa_1$ ($\equiv\Delta\kappa$) could be considered as a measure of the deviation of a signal from that having a uniform distribution.

V. THE ENTROPY

The derivative of the function $\langle\chi^q\rangle-\langle\chi\rangle^q$, with respect to q, i.e., $\langle\chi^q\ln\chi\rangle-\langle\chi\rangle^q\ln\langle\chi\rangle$, is plotted in Fig. 8(b) versus q. We may see again a classification, but here we pay attention to the region around $q=1$. The term $\langle\chi\ln\chi\rangle-\langle\chi\rangle\ln\langle\chi\rangle$ is reminiscent of an excessive entropy (see pp. 26–28 of Ref. [3], but recall that the usual expressions of the thermodynamic potentials, in terms of macroscopic variables, break down far from equilibrium [3] and the behavior of entropy is still a matter of intensive investigation [29]). In such a simplified scheme, the ICFMC lies just in the boundary between the SES activities (critical dynamics) and the AN (more "disorder").

Let us now further study the aforementioned values of the quantity $\langle\chi\ln\chi\rangle-\langle\chi\rangle\ln\langle\chi\rangle$. For reasons of brevity, this will be hereafter called entropy and labeled S, i.e., $S\equiv\langle\chi\ln\chi\rangle-\langle\chi\rangle\ln\langle\chi\rangle$. It consists of two terms $S_\chi\equiv-\langle\chi\ln\chi\rangle$ and $S_{\langle\chi\rangle}\equiv-\langle\chi\rangle\ln\langle\chi\rangle$ and hence $S=-S_\chi+S_{\langle\chi\rangle}$. Considering that $(d/dx)[x^2/4-(x^2/2)\ln x]=-x\ln x$ and taking into account that for a uniform (u) distribution $\langle\chi\rangle=1/2$, we find $S_{\chi,u}=1/4$ and $S_{\langle\chi\rangle}=(1/2)\ln 2\approx0.3466$. Thus, the entropy S_u of the uniform distribution has the value $S_u\approx0.0966$. In Ref. [11], we study the expected values, along with their vari-

ances, for κ_1 and S for a uniform distribution as a function of the number of the high-level states N_h. The values of κ_1 and S for all the SES activities and AN of Fig. 1 are shown in Table I. The fact that only $n5$ among AN seems to have a smaller entropy than S_u ($S[n5]=0.091\pm0.011$) might be understood as follows: For $n5$, we have $N_h\approx400$ for which Ref. [11] reveals that the aforementioned value of 0.091 differs *only* by an amount smaller than one standard deviation from S_u.

Therefore the three types of electric signals appear to be classified as follows: AN have an entropy larger than that of the uniform distribution, i.e., $S>S_u$, while the SES activities
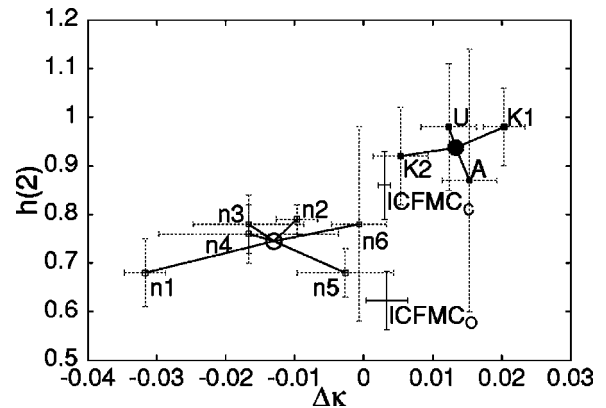

FIG. 9. Combined results of the analyses made in the natural time domain: SES activities—$K1$, $K2$, A, U (full squares), AN—$n1$ to $n6$ (open squares). The $h(2)$ values were obtained by MF-DFA (Table I). For ICFMC, the power-law exponents reported in Ref. [32] for the open states (labeled ICFMC$_o$) and the closed states (labeled ICFMC$_c$) were used. The thick straight lines show the two groups resulting from the application [11] of the K-MEANS clustering algorithm (the full and open circles correspond to the centroids of the two groups).

exhibit S values smaller than S_u. As for the ICFMC, the S value lies very close to S_u.

VI. DISCUSSION

We first discuss the results of the wavelet transform in the natural time domain. Recalling that $h(2)=H$, the results (see the third column in Table I) could be understood in the following context: The fact that the Hurst exponent H for the SES activities (critical dynamics [3]) is close to unity, may reflect [10] that the intensity of their long-range correlations is appreciably stronger than that for the AN (whose H lies approximately in the range 0.69–0.86). This finding is consistent with the results deduced [10] by MF-DFA in the natural time domain, which for the sake of comparison are also inserted in the second column of Table I.

We now plot in Fig. 9 the $h(2)$ values versus the deviations from the uniform behavior ($\Delta\kappa$ values) defined in Sec. IV. A more elaborated classification of the results depicted in this figure can be obtained through a clustering algorithm. We used [11] here a K-MEANS type [30] which is a least-squares partitioning method allowing users to divide a collection of objects into K groups (e.g., see Sec. 8.8 of Ref. [31]). This clustering algorithm reveals [11] the existence of *two* groups: the first group includes the four SES activities, while the second the six AN $n1$–$n6$, if the $h(2)$ values of MF-DFA (Table I) are used. *Two* groups, i.e., one including the three SES activities $K1$, $K2$, and U and the other consisting of the five AN $n1$–$n5$, are again found if we take into account the $h(2)$ values determined by the wavelet transform method, instead of MF-DFA (Table I).

In summary, the following classification seems to emerge. First, the SES activities, which correspond to large $\Delta\kappa$ values ($\Delta\kappa>0$), are characterized by the strongest "memory" (large H, close to unity); both their $\Delta\kappa$ and $h(2)$ values are consistent with those expected for a critical behavior. Second, AN simultaneously have smaller $\Delta\kappa$ values ($\Delta\kappa\lesssim 0$) and weaker memory (their H values are markedly smaller than unity). Third, concerning the ICFMC, the values related with the closed states, which have been found [32] to exhibit the stronger memory (between the two states, i.e., closed and open), seem to lie in the boundary between the aforementioned two regimes.

Finally, we emphasize that the randomly "shuffled" series of *all* the three types of electric signals investigated lead to $H\approx 0.5$ (simple random behavior) and $\Delta\kappa\approx 0$. These two values are internally consistent, because in the shuffling procedure the values are put into random order, and thus all correlations (memory) are destroyed.

VII. CONCLUSIONS

Three types of electric signals of dichotomous nature were studied: ICFMC, SES activities, and AN. Their analysis led to the following main conclusions, which simultaneously provide rules for the practical problem of the distinction between SES activities and AN (cf. the subscripts below designate each class of signals).

(1)The qth order fluctuation function $\langle\chi^q\rangle-\langle\chi\rangle^q$ versus q, seems to allow a classification of the three types of signals as follows: For q values approximately between 1 and 2, the curve of ICFMC lies in the boundary between the other two types of signals; specifically, the AN have values larger than those of the ICFMC, while the SES activities are characterized by smaller values, i.e.,

$$\langle\chi^q\rangle-\langle\chi\rangle^q|_{SES}<\langle\chi^q\rangle-\langle\chi\rangle^q|_{ICFMC}\lesssim\langle\chi^q\rangle-\langle\chi\rangle^q|_{AN}$$

in the range $1<q\leq 2$ (for the special case $q=2$, elaborated in Ref. [10], this rule reveals $\kappa_{1,SES}<\kappa_{1,ICFMC}\lesssim\kappa_{1,AN}$, where $\kappa_{1,ICFMC}\approx 0.080$).

(2)The entropy, i.e., the quantity $S=\langle\chi\ln\chi\rangle-\langle\chi\rangle\ln\langle\chi\rangle$, may also serve for a classification: The SES activities have an entropy smaller than that of the uniform (u) distribution, i.e., $S<S_u$, while AN exhibit S values larger than S_u:

$$S_{SES}<S_{ICMFC}\lesssim S_{AN},$$

where the value of S_{ICFMC} is comparable to that of the uniform distribution, i.e., $S_{ICFMC}\approx 0.096\approx S_u$.

(3)The application of the wavelet transform in the conventional time frame does not seem to provide a distinction between SES activities and AN, but does so in the natural time domain. Recall that the same conclusion was drawn in Ref. [10], where DFA and MF-DFA had been employed. The following rule emerges (in the natural time domain):

$$H_{AN}\lesssim H_{ICFMC,c}<H_{SES},$$

where H_{SES} is close to unity and $H_{ICFMC,c}\approx 0.86$, while $H_{AN}\lesssim 0.86$.

Finally, the fact that *both* SES activities and AN (which are non-Markovian time series, as it results from their quantitative global measure G as well as their dwell-time distributions) give [10] on short time scales a DFA exponent $1\leq\alpha\leq 1.5$ was illuminated in this paper. We showed that in the conventional time domain even a Markovian dichotomous time series can, in short time scales, result in α values in the range $1\leq\alpha\leq 1.5$; in general, any signal with a high frequency spectrum as given in Eq. (3) will lead to the same scaling behavior of $F_{DFA}(\Delta t)$ for small time lags Δt.

Note added in proof. In Ref. [5], it has already been noticed that the entropy S (defined here in Sec. V) can have useful applications to electrocardiograms (ECG). Actually, it has been recently shown that the standard deviation δS, when calculating S by a sliding window of short length, can reveal important properties in ECG. Details will be published elsewhere.

[1] A. Fuliński, Z. Grzywna, I. Mellor, Z. Siwy, and P.N.R. Usherwood, Phys. Rev. E **58**, 919 (1998).

[2] Z. Siwy, M. Ausloos, and K. Ivanova, Phys. Rev. E **65**, 031907 (2002).

[3] P. Varotsos and K. Alexopoulos, *Thermodynamics of Point Defects and their Relation with Bulk Properties* (North-Holland, Amsterdam, 1986).

[4] P. Varotsos, N. Sarlis, and E. Skordas, Proc. Jpn. Acad., Ser. B: Phys. Biol. Sci. **77**, 93 (2001).

[5] P. Varotsos, N. Sarlis, and E. Skordas, Practica Athens Academy **76**, 294 (2001).

[6] P. Varotsos, N. Sarlis, and E. Skordas, Acta Geophys. Pol. **50**, 337 (2002).

[7] P. Varotsos, *The Physics of Seismic Electric Signals* (TERRA-PUB, Tokyo, in press).

[8] S. Uyeda, T. Nagao, Y. Orihara, T. Yamaguchi, and I. Takahashi, Proc. Natl. Acad. Sci. U.S.A. **97**, 4561 (2000).

[9] S. Uyeda, M. Hayakawa, T. Nagao, O. Molchanov, K. Hattori, Y. Orihara, K. Gotoh, Y. Akinaga, and H. Tanaka, Proc. Natl. Acad. Sci. U.S.A. **99**, 7352 (2002).

[10] P.A. Varotsos, N.V. Sarlis, and E.S. Skordas, Phys. Rev. E **67**, 021109 (2003).

[11] See EPAPS Document No. E-PLEEE8-68-116309 for additional information. A direct link to this document may be found in the online article's HTML reference section. The document may also be reached via the EPAPS homepage (http://www.aip.org/pubservs/epaps.html) or from ftp.aip.org in the directory /epaps/. See the EPAPS homepage for more information.

[12] P.A. Varotsos, N.V. Sarlis, and E.S. Skordas, Phys. Rev. E **66**, 011902 (2002).

[13] S. Mercik and K. Weron, Phys. Rev. E **63**, 051910 (2001).

[14] C.-K. Peng, S.V. Buldyrev, S. Havlin, M. Simons, H.E. Stanley, and A.L. Goldberger, Phys. Rev. E **49**, 1685 (1994).

[15] S.V. Buldyrev, A.L. Goldberger, S. Havlin, R.N. Mantegna, M.E. Matsa, C.-K. Peng, M. Simons, and H.E. Stanley, Phys.

[16] P. Talkner and R.O. Weber, Phys. Rev. E **62**, 150 (2000).

[17] Z. Chen, P.C. Ivanov, K. Hu, and H.E. Stanley, Phys. Rev. E **65**, 041107 (2002).

[18] P.C. Ivanov, L.A.N. Amaral, A.L. Goldberger, S. Havlin, M.G. Rosenblum, H.E. Stanley, and Z.R. Struzik, Chaos **11**, 641 (2001).

[19] J.F. Muzy, E. Bacry, and A. Arneodo, Int. J. Bifurcation Chaos Appl. Sci. Eng. **4**, 245 (1994).

[20] A. K. Louis, P. Maas, and A. Rieder, *Wavelets: Theory and Applications* (Wiley, New York, 1997).

[21] P. Abry, P. Flandrin, M. S. Taqqu, and D. Veitch, in *Self Similar Network Traffic Analysis and Performance Evaluation*, edited by K. Park and W. Willinger (Wiley, New York, 2000).

[22] B. Audit, E. Bacry, J. Muzy, and A. Arneodo, IEEE Trans. Inf. Theory **48**, 2938 (2002).

[23] R. Weber and P. Talkner, J. Geophys. Res. [Atmos.] **106**, 20131 (2001).

[24] J. Kantelhardt, S.A. Zschiegner, E. Koscielny-Bunde, A. Bunde, S. Havlin, and H.E. Stanley, Physica A **316**, 87 (2002).

[25] A.M. Berezhkovskii and G.H. Weiss, Physica A **303**, 1 (2002).

[26] E. Bacry, computer code LASTWAVE available from URL http://www.cmap.polytechnique.fr/~bacry/LastWave

[27] D. Veitch, P. Abry, and P. Chainais, computer codes WAVELET ESTIMATION TOOLS available from URL http://www.emulab.ee.mu.oz.au/~darryl

[28] After checking several other Daubechies wavelets of higher order.

[29] B. Gaveau, K. Martinás, M. Moreau, and T. Tóth, Physica A **305**, 445 (2002).

[30] P. Legendre, computer code K-MEANS available from URL http://www.fas.umontreal.ca/BIOL/legendre

[31] P. Legendre and L. Legendre, *Numerical Ecology* (Elsevier, Amsterdam, 1998).

[32] Z. Siwy, S. Mercik, K. Weron, and M. Ausloos, Physica A **297**, 79 (2001).